Transactions on Electrical and Electronic Materials (2024) 25:674–684
https://doi.org/10.1007/s42341-024-00547-y

Online ISSN 2092-7592
Print ISSN 1229-7607

REGULAR PAPER

# Molybdenum Disulphide and Titanium Dioxide Nanocomposite Based fast Humidity Sensor with Linear Response over wide Humidity Range

**Arshad Majeed[1] · S. M. T. Kazmi[1] · A. Zafar[2] · Hira Tasqeen[3] · M. A. Rafiq[1]**

Received: 9 January 2024 / Revised: 9 April 2024 / Accepted: 12 May 2024 / Published online: 24 May 2024


## Abstract

A humidity sensor based on $MoS_2/TiO_2$ nanocomposite prepared by solid state reaction method is presented in this work. X-ray diffraction (XRD) confirms the formation of nanocomposite consisting of irregular shaped nanoparticles of different sizes (60 –200 nm). Energy Dispersive Spectroscopy (EDS) confirms the presence of Titanium, Molybdenum, Sulphur, and Oxygen in the nanocomposite. Humidity sensing characteristic of $MoS_2/TiO_2$ nanocomposite are studied at room temperature from 11 to 97% relative humidity (RH) using AC impedance spectroscopy. The response and sensitivity of $MoS_2/TiO_2$ nanocomposite sensor are calculated from AC impedance data. The values of response and sensitivity turn out to be 86% and ∼13 k$\Omega/\%RH$ , respectively at 100 Hz. The nanocomposite sensor shows response and recovery time of ∼38s and ∼7s respectively with good repeatability. The sensor response remains stable for 30 days. Moreover, RH effect on AC conductivity and complex electric modulus of $MoS_2/TiO_2$ nanocomposite are also investigated.

## Highlights

- Solid state reaction method is employed to prepare $MoS_2/TiO_2$ nanocomposite.
- Nanoparticle of irregular size ∼ (60 –200 nm) confirmed by XRD.
- EDS analysis confirms the presence of Molybdenum, Titanium, Sulphur and Oxygen in nanocomposite.
- AC impedance spectroscopy is studies from 11 to 97% RH for characterization at room temperature.
- Response (86%), sensitivity (∼13kΩ)/%RH is achieved at 100 Hz.
- We found response time ∼38s and recovery time ∼7s with overall good repeatability and stability.
- Impact of RH on AC conductivity and complex electric modulus is explored.

✉ M. A. Rafiq
aftab@cantab.net

[1] Condensed Matter Physics Laboratories, Department of Physics and Applied Mathematics, Pakistan Institute of Engineering and Applied Sciences (PIEAS), P. O. Nilore, Islamabad 4650, Pakistan

[2] Central Analytical Facility Division (CAFD), PINSTECH, Islamabad, Pakistan

[3] Department of Chemistry, COMSATS university, Islamabad, Pakistan

**Graphical Abstract**

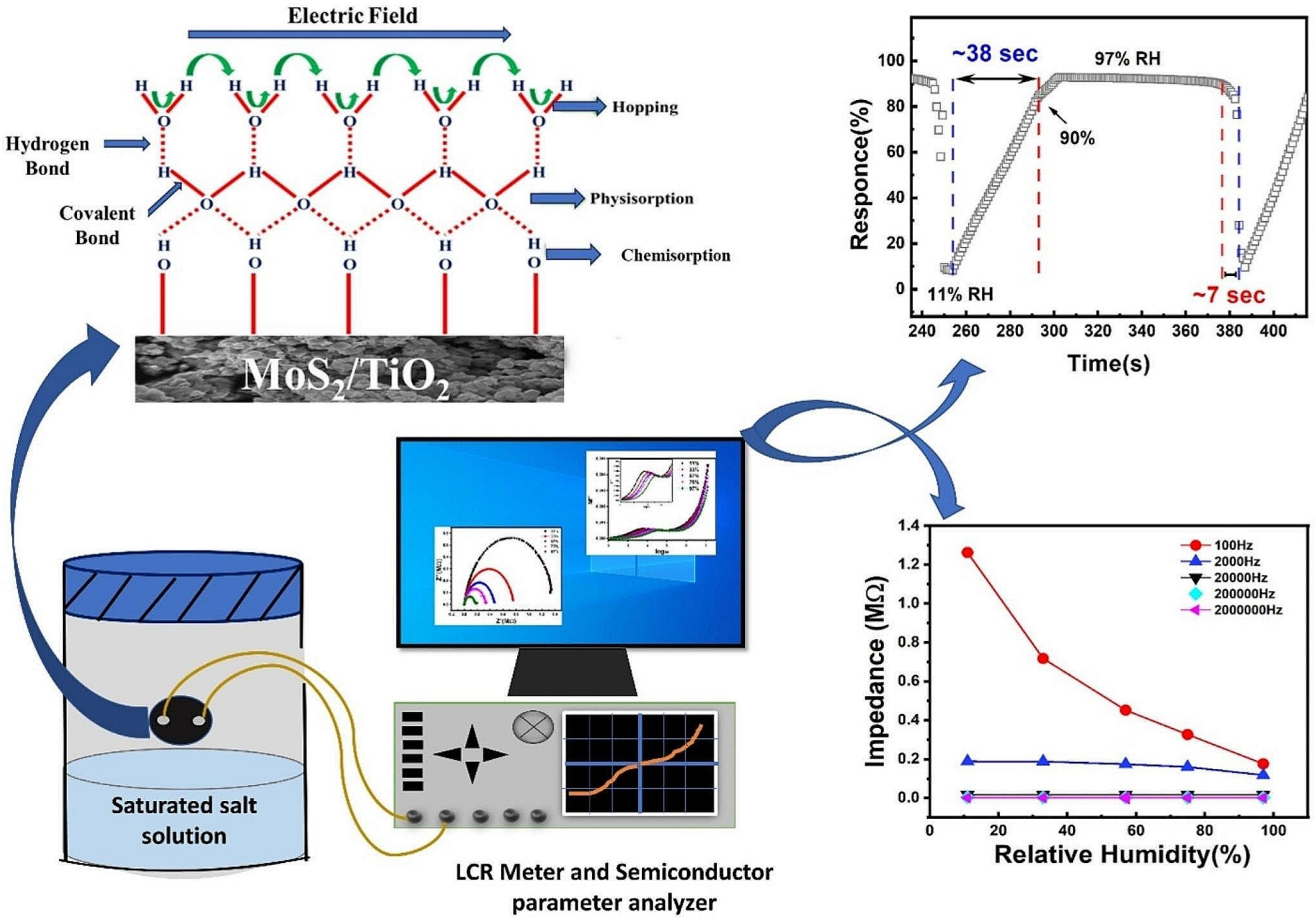


**Keywords** Nanocomposites · Impedance · Humidity sensor · AC conductivity · Molybdenum disulphide · Titanium dioxide

## 1 Introduction

In recent years, there has been an increasing trend of utilizing nanocomposite technologies to fabricate ultra-low-cost electronic components [1]. Numerous industrial processes require precise humidity control, such as chemical purification of gases, paper production and textiles, and food processing [2]. For these applications a humidity sensor with higher sensitivity, linear response, fast response and recovery times, chemical and physical stability, cost-effectiveness, and a broad operating humidity range is currently high in demand. There are different transduction techniques, including impedance, capacitance, resistance, surface acoustic wave (SAW), optical fiber, and quartz crystal microbalance (QCM), have been employed to develop humidity sensors. Among these, impedance type humidity sensors are low power consumption sensors [3]. Various materials have been investigated for their humidity sensing capabilities, including polymers [4], ceramics, metal oxides semiconductor [5], carbon nanomaterials [6], cellulose [7], and transition metal dichalcogenides (TMDCs) [8]. TMDCs like Molybdenum disulfide ($MoS_2$) with each layer comprising molybdenum atoms sandwiched between two layers of sulphur atoms exhibits exceptional properties, due to large specific surface area, high electron mobility and carrier's concentration. $MoS_2$ based humidity sensors have large surface-to-volume ratio. However, $MoS_2$ has electrochemical activity at its edge plane while the matrix plane has chemical inertia which causes poor performance for humidity sensing [9]. To overcome shortcoming of $MoS_2$ sensing performance, researchers have proposed combing it with other sensing material to make composite or doping. Specially, TMDCs composites with metal oxides have been reported to be promising method for improving humidity sensing performance of TMDCs. High k Metal oxides such as $TiO_2$, $ZrO_2$ and $HfO_2$ are useful, sense humidity due to

their ability to generate defects via doping or composite formation which improve overall water adsorption ability that results in improvement in sensitivity of the sensor. These materials show significant changes in their impedance over a wide humidity range indicating the suitability of these materials for precise humidity sensing measurement [10].

Jiahao Yao reported humidity sensor based on (In, Nb) Doped $HfO_2$ [10]. Zang et al. reported high performance impedance type humidity sensor based on $SnS_2/TiO_2$ [11]. Zhang et al. reported capacitive type $SnO_2$ modified $MoS_2$ with ultrahigh sensitivity [12]. Li et al. reported that composite $MoS_2$/CuO humidity sensor exhibits enhanced response/recovery time and sensitivity [13]. Ze et al. presented a fast humidity sensor based on ZnO quantum dot modified $MoS_2$ [14]. Burman et al. [15] reported ZnO/$MoS_2$ based enhanced humidity sensing performance. In view of above, we have prepared $TiO_2$ and $MoS_2$ nanocomposites as high k oxide $TiO_2$ possesses super hydrophilicity, stability, high sensitivity, biocompatibility, mechanical stability, chemical stability and thermal stability [16]. While the presence of $Ti^{3+}$ defect sites in $TiO_2$ renders its hydrophilicity, making the dissociative adsorption of water [17]. From various phases of $TiO_2$, anatase phase of $TiO_2$ has been found as favourable phase for humidity sensing, owing to its higher water adsorption capacity [18]. Moreover, physiosorbed water is easy to desorb at anatase phase compared to rutile phase [19].

In this study we prepared $MoS_2/TiO_2$ nanocomposite humidity sensor. It was tested using complex impedance spectroscopy and sensor parameters such as percentage response, sensitivity, stability, and repeatability were extracted from impedance data at room temperature. The response and recovery times were measured from DC measurements. The effect of RH on the AC conductivity and complex electric modulus of the sensor was also examined.

## 2 Experimental

For the synthesis of $MoS_2/TiO_2$ nanocomposite, solid-state reaction method was employed. The precursors ammonium molybdate tetrahydrate, thiourea, and $TiO_2$ were purchased from sigma Aldrich with 99.9% purity. To start the synthesis process, ammonium molybdate tetrahydrate, thiourea, and $TiO_2$ were mixed in 1:2:1 ratio, respectively and ground for 20 min to get a fine powder. The resulting fine powder was then transferred to a crucible. The crucible containing the powder was placed in a tube furnace under Argon flow at 650˚C for 6 h. The heating and cooling rate was 5˚C/min. The obtained $MoS_2/TiO_2$ nanocomposite powder after heating was allowed to cool at room temperature. The nanocomposite powder was ground again to obtain fine powder that was used for humidity sensing experiments. The synthesis process of $MoS_2/TiO_2$ nanocomposite is shown schematically in Fig. 1.

To perform humidity sensing experiments $MoS_2/TiO_2$ nanocomposite powder was pressed to form pellets in hydraulic press under a load of ~ 3 ton. The pellets diameter and thickness were 13 mm and 1 mm respectively. Electrical contacts on one side of the pellets were formed using silver paste. The separation between the contacts was 8 mm. To increase adhesion of the electrical contacts with pellets, the pellets were sintered at 60 ˚C for 60 min.

To test the $MoS_2/TiO_2$ sensor, variation of AC impedance of sensor at different RH were recorded using Agilent E4980A LCR meter. The response recovery times of the sensor were measured using Agilent 4156 C parameter

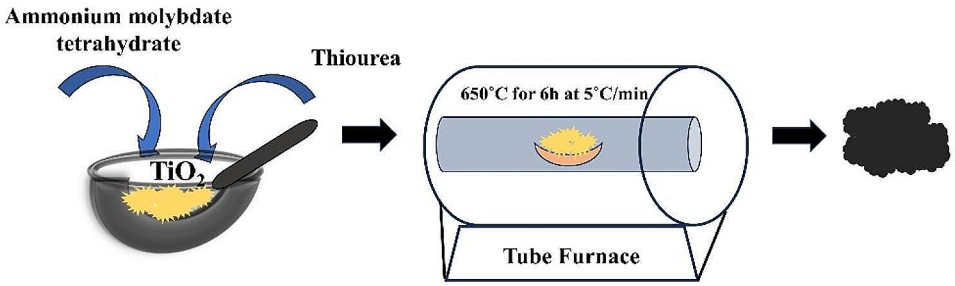


**Fig. 1** Systematic growth of $MoS_2/TiO_2$ nanocomposite

analyser. Different RH in small chambers were achieved using saturated salt solutions kept in chamber for 24 h. The saturated salt solution of Potassium Sulphate ($K_2SO_4$), Sodium Chloride (NaCl), Sodium Bromide (NaBr), Magnesium Chloride ($MgCl_2$) and Lithium Chloride (LiCl) yielded RH 97.6%,75.3%,57.6%,33% and 11% respectively [20].

## 3 Result and Discussion

XRD analysis was done to investigate the crystallinity, phase composition, and purity of the $MoS_2/TiO_2$ nanocomposite using PANalytical X'pert Pro diffractometer. This diffractometer employs a Cu-Kα radiation source with wavelength 1.540 Å. The XRD was performed for 2θ values ranging from 20˚ to 80˚. The XRD pattern of $MoS_2/TiO_2$ nanocomposite is shown in Fig. 2. The peaks corresponding to standard XRD pattern of pure $MoS_2$ and $TiO_2$ are present in pattern. All diffraction peaks for $MoS_2$ match with the standard JCPDS card (00-002-0132) with hexagonal phase and space group P63/mmc. The lattice parameters are a = 3.15 Å, b = 3.15 Å, and c = 12.30 Å for $MoS_2$ constituent of the nanocomposite. The peaks at 2θ equal to 32.9˚ and 58.5˚ correspond to the (100) and (110) planes. Similarly, the diffraction peaks of $TiO_2$ are present at 2θ equal to 25.2˚, 37.8˚, 48.0˚ and 53.7˚ corresponding to (101), (103), (200) and (105) planes respectively. The lattice parameters are a = 3.73 Å, b = 3.73 Å, and c = 9.37 Å for $TiO_2$ constituent of the nanocomposite. These peaks match with JCPDS card (00-001-0562). Here the anatase $TiO_2$ has tetragonal phase with space group 141/amd. The crystallite size was calculated using equation:

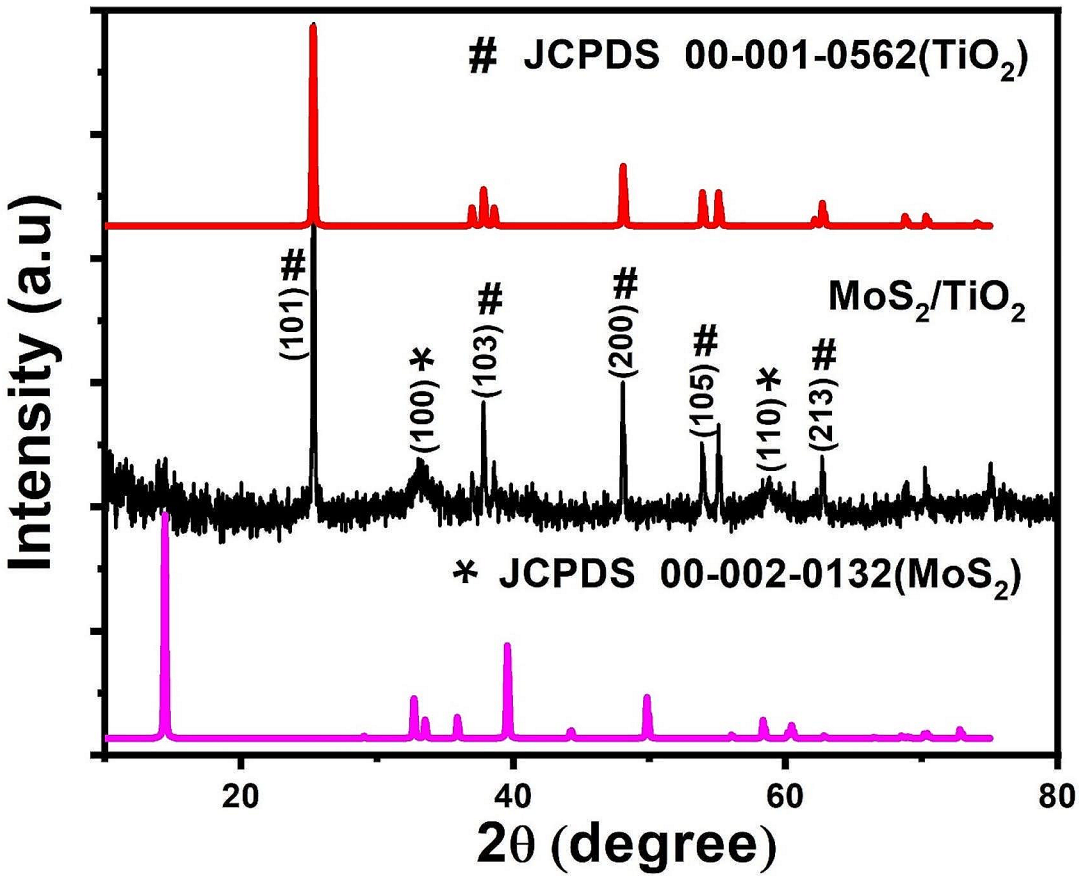


**Fig. 2** XRD spectrum of $MoS_2/TiO_2$ nanocomposite

$$L = \frac{K\lambda}{\beta Cos\theta} \quad (1)$$

where $K$ is the Scherrer constant whose value ranges from 0.68 to 2.08. The $\lambda = 1.5406$ Å is the wavelength of *Cu-Kα* X-ray radiation source, $\beta$ is the line broadening at FWHM of the XRD peaks, and $\theta$ is Bragg's angle. The calculated crystallite size of the $MoS_2/TiO_2$ nanocomposite is 57.65 nm.

Surface morphology of as synthesized sample of $MoS_2/TiO_2$ nanocomposite was examined using SEM. Figure 3(b) shows SEM image of $MoS_2/TiO_2$ nanocomposite. The nanocomposite consists of irregular shaped nanoparticles of different sizes. The nanoparticle size ranges from ~ 60–200 nm with average nanoparticle size ~ 117 nm as shown in Fig. 3(c). EDS spectrum confirms the presence of Mo, S, Ti and O as shown in Fig. 3(a). This confirms the formation of $MoS_2/TiO_2$ nanocomposite without presence of any impurities. The presence of carbon in EDS spectrum comes from the carbon tape that was used during EDS measurements.

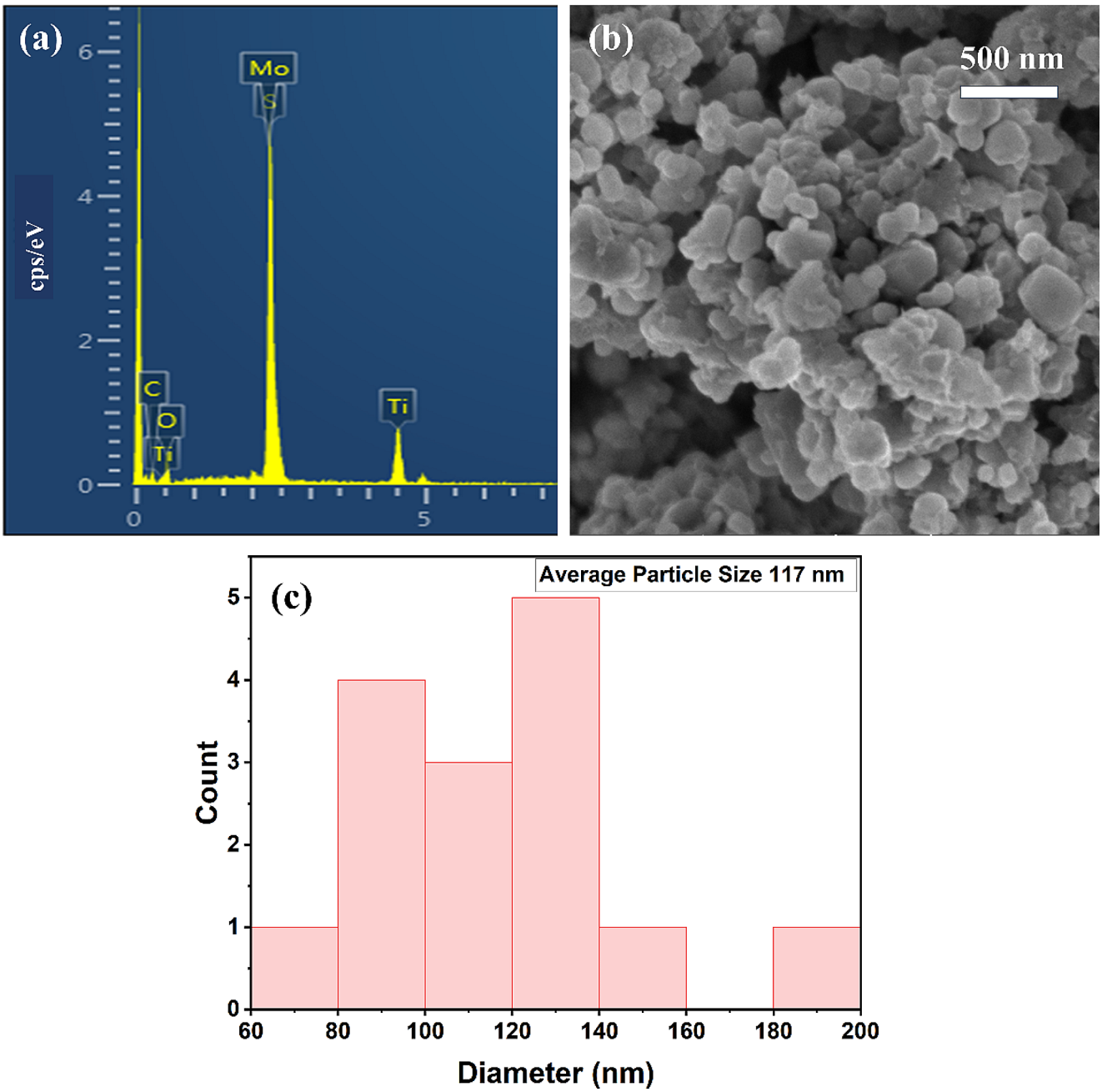


**Fig. 3** **(a)** EDS spectrum of $MoS_2/TiO_2$ nanocomposite **(b)** Scanning electron micrograph of $MoS_2/TiO_2$ nanocomposite **(c)** Particle size distribution histogram of nanocomposite $MoS_2/TiO_2$

Complex impedance spectroscopy was used to investigate humidity sensing of $MoS_2/TiO_2$ nanocomposite. Measurements were performed under ambient condition at 1.5 V AC signal ranging from 20 Hz to 2 MHz Complex impedance is defined as $Z^*= Z' + Z''$ where $Z'$ and $Z''$ are real and imaginary part of the impedance, respectively. Figure 4(a) shows the $Z'$ vs. $Z''$ plot of $MoS_2/TiO_2$ nanocomposite. Frequency is increasing from right to left on real axis. The diameter of the semicircles at different RH gives bulk resistance of $MoS_2/TiO_2$. At higher humidity level the spure can be observed at the end of the semicircles. That indicate ionic conduction is more prominent than electronic conductivity [21]. Due to hydrophilic nature of $MoS_2/TiO_2$ nanocomposite water molecules adsorbed on surface of material, which play important role in altering its bulk resistance. Overall, with increasing RH level from 11 to 97% the bulk resistance of $MoS_2/TiO_2$ decreases from 1261.9 KΩ to 175.8 KΩ, at 100 Hz and 1.5 KΩ to1.0 KΩ at 2 MHz. This

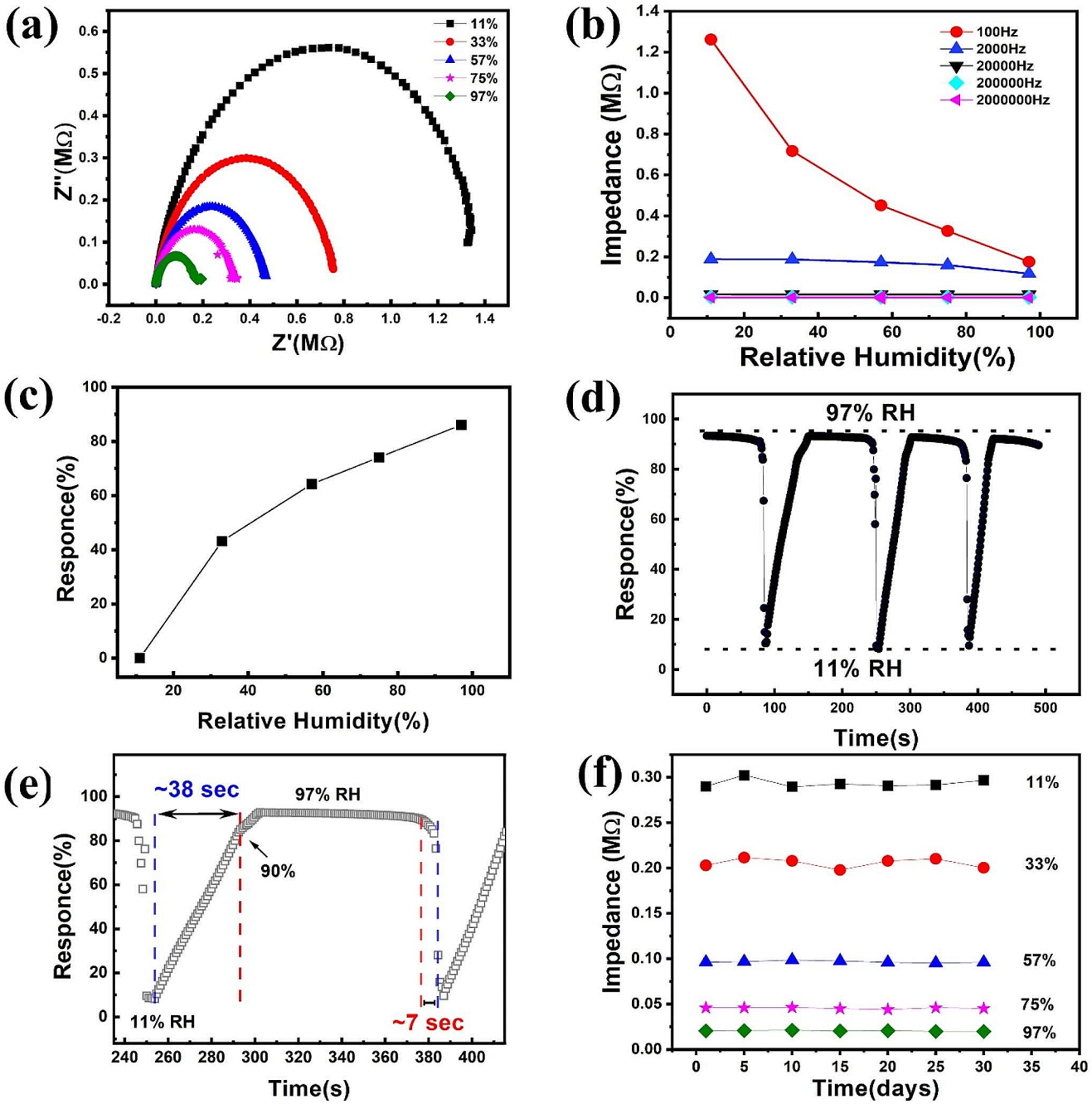


**Fig. 4** **(a)** $Z'$ vs. $Z''$ plot of $MoS_2/TiO_2$ nanocomposite **(b)** Impedance vs. RH at different frequencies of $MoS_2/TiO_2$ nanocomposite **(c)** Response of $MoS_2/TiO_2$ nanocomposite sensor **(d)** Repeatability of $MoS_2/TiO_2$ nanocomposite **(e)** Response and recovery curve of $MoS_2/TiO_2$ nanocomposite **(f)** Stability of $MoS_2/TiO_2$ nanocomposite

change in resistance is larger at lower frequencies as shown in Fig. 4(b). The non-linear behaviour of impedance with RH at lower frequencies is due to defects and surfaces prodigious effects [22]. Higher frequencies suppressed these effects, as linear behaviour of impedance can be observed in Fig. 4(b) at higher frequency. Sensitivity of device can be calculated by using [23];

$$Sensitivity = \frac{\Delta\,(Impedence)}{\Delta\,(\%RH)} \tag{2}$$

Sensitivity of $MoS_2/TiO_2$ nanocomposite in RH range 11–97% was 12.62 kΩ/$\%RH$, 0.82 kΩ/$\%RH$ and 0.005 kΩ/$\%RH$ at 100 Hz, 2 kHz and 2 MHz respectively.

Percentage response of the sensor is given as;

$$Response\,(\%) = \frac{R_{11\%} - R_{high\%}}{R_{11\%}} \times 100 \tag{3}$$

Where $R_{11\%}$ is the resistance at 11% RH and $R_{high\%}$ at any higher RH level. Percentage response of the sensor was calculated as 86%, 74%, 64% and 43% at 97%, 75%, 57% and 33% RH level respectively as shown in Fig. 4(c). Response and recovery time are also the important sensor's parameters. Response time is defined as time required to change impedance up to 90% of its maximum value while adsorption and recovery time is time required to change impedance up to 90% of its maximum value while desorption. From Fig. 4(e) $MoS_2/TiO_2$ nanocomposite shows the response and recovery time of ~38s and ~7s respectively by changing the RH value between 11% and 97%. Due to physisorption and chemisorption phenomenon desorption process is faster than adsorption process. That results in the shorter recovery time of the $MoS_2/TiO_2$ sensor compared to its response time. At low RH level chemisorption is more dominant because two hydroxyls of water form a double bond with surface and become immobile. Physisorption is dominant at higher RH level that involves Van Der Walls bonding between the surfaces. This interaction is weaker than chemical bonding hence become more moveable charges result in shorter recovery time [24]. $MoS_2/TiO_2$ nanocomposite sensor shows good repeatability over three consecutive cycles with minimum deviation as shown in Fig. 4(d).

The humidity sensing parameters of $MoS_2/TiO_2$ nanocomposite humidity sensor were compared with those of other nanocomposite based humidity sensors, as listed in Table 1. Analysis of the data presented in Table 1 validates that our findings are better or comparable with those of previously reported humidity sensors based on nanocomposites.

Stability of sensor was checked for one month with the gap of 5 days under humidity level 11–97%. A little change in the value of impedance was observed during whole month as shown in Fig. 4(f).

The effect of RH on AC conductivity, and modulus (M*) of $MoS_2/TiO_2$ nanocomposite was also studied. AC conductivity $(\sigma_{a\cdot c})$ with different RH as function of frequency is shown in Fig. 5(a). Electrical conductivity provides valuable insights into the behaviour of electric charge flow within this system. AC conductivity of $MoS_2/TiO_2$ nanocomposite was calculated from complex impedance by using;

$$\sigma_{a\cdot c} = \left(\frac{Z'}{(Z')^2 + (Z'')^2}\right)\frac{d}{A} \tag{4}$$

Here $A$ and $d$ are the cross-sectional area and the thickness of the sensor, respectively. The AC conductivity also shows dependence on frequency and this behaviour can be described using a universal power law equation [25].

$$\sigma\,(\omega) = A\omega^n + \sigma\,(0) \tag{5}$$

σ(ω) signifies the AC conductivity at a specific angular frequency ω, '$n$' represents a frequency exponent, '$A$' stands for the AC conductivity factor, and 'σ(0)' corresponds to DC conductivity $(\sigma_{d\cdot c})$. It is noteworthy that the value of $n$ depends upon the RH. Its value lies between 0 and 1, for $MoS_2/TiO_2$ its value increases from 0.01 to 0.02 when RH changes from 11 to 97%. We observe that the conductivity within this system displays two distinct regions the initial

**Table 1** Comparison of different nanocomposite humidity sensor's parameters

| Sensing Material | Response Time | Recovery Time | Method | Type | Range | Sensitivity | Response | ref |
|---|---|---|---|---|---|---|---|---|
| $SnO_2$-$TiO_2$ | 19.1 | 131 | RF sputtering deposition | Impedance | 10–95 | 12.37MΩ/%RH | - | [8a] |
| $MoS_2$/ZnO | 138 | 266 | Chemical bath deposition | Resistive | 35–85 | - | 301% | [15] |
| $SnS_2$ /$TiO_2$ | 150 | 38 | LbL self-assembly | Impedance | 11–97 | 442000Ω/%RH | - | [11] |
| CeO2/molecular sieves | 9 | 80 | Simple method | Impedance | 11–95 | $1.04\times10^5$ Ω/%RH | - | [32] |
| SnO2/TiO2 | 18 | 27 | Solid state reaction | Impedance | 15–65 | - | - | [33] |
| $MoS_2/TiO_2$ | 38 | 7 | Solid state reaction | Impedance | 11–97 | 12.62kΩ/%RH | 86% | This work |

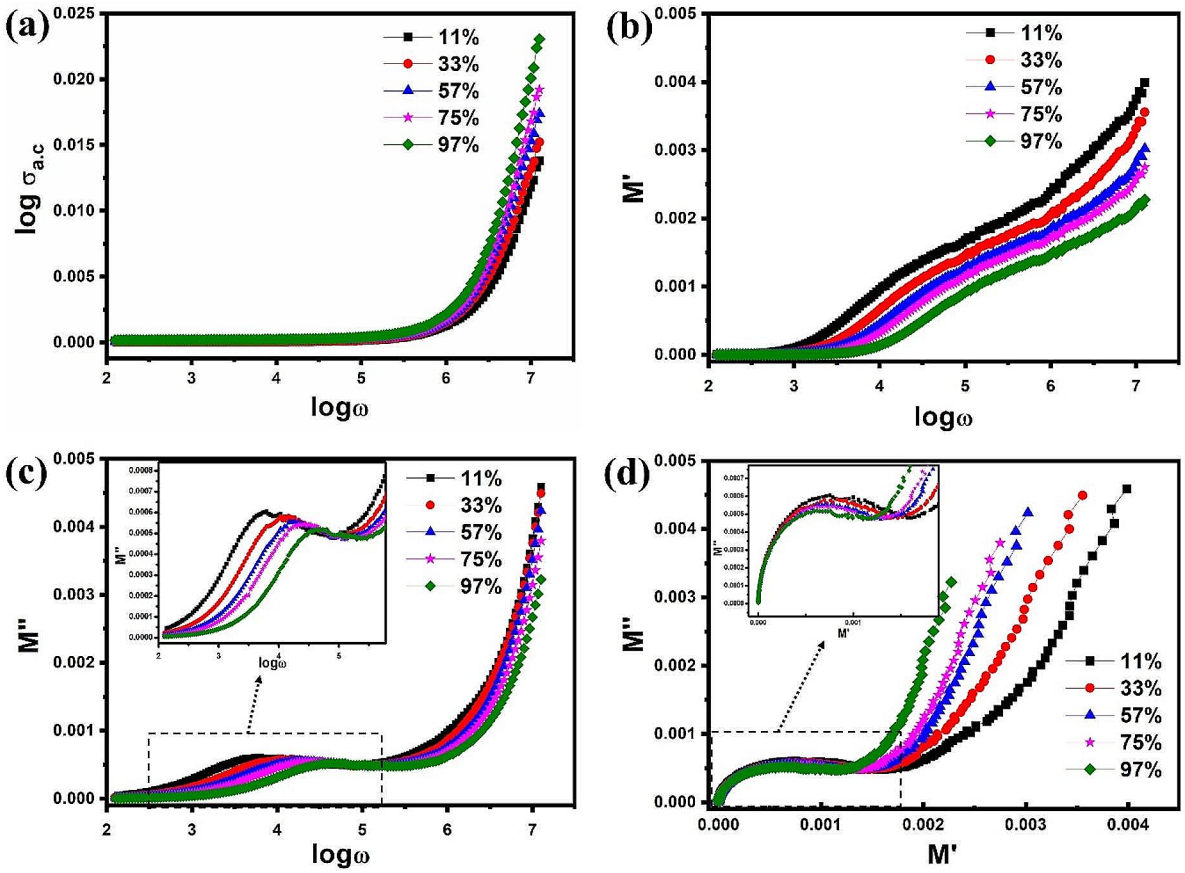


**Fig. 5** **(a)** AC conductivity vs. log ω with different RH **(b)** $M'$ vs. log ω with different RH **(c)** M″ vs. $\log_{\omega}$ with different RH **(d)** Nyquist plot M′ vs. M″

region is characterized by a plateau, (up to $10^5$ Hz) which is associated with $(\sigma_{d\cdot c})$ at lower frequencies. This plateau arises due to the polarization of electric charge at the interface between the electrode and the specimen. The second region, situated at higher frequencies, exhibits frequency dispersion, corresponding to the $\sigma_{a\cdot c}$. In this region, the migration of charge takes place under the influence of the applied electric field.

Complex electric modulus allows us to understand the relaxation process and bulk response of material by differentiating local response of defects from electrode effect. complex modulus ($M^*$) is defined as [26].

$$M^*(\omega) = \frac{1}{\epsilon^*(\omega)} = M' + iM'' = i\omega C_o Z^* \tag{6}$$

Here $M\prime = i\omega C_o Z\prime$ is real part, $M\prime\prime = i\omega C_o Z\prime\prime$ is imaginary part of complex modulus and $C_o = \frac{A\epsilon_o}{d}$ is geometrical capacitance. Figure 5(b) shows graph between real part of modulus ($M_{,}$) as a function of frequency and humidity. At low frequency $M_{,}$ has small values indicating presence of electrode polarization which mask the bulk relaxation process, at higher frequency its value reaches at maximum value. The value of M′ increases with increasing frequency, but its value decreases with increasing RH. Dispersion in M′ with increasing frequency can be due to conduction of short range charge carriers [27]. Transition from low to high value of M′ with increasing frequency suggest us a relaxation process which must be observed in M″ vs. $\log_{\omega}$ curve. Graph between M″ vs. $\log_{\omega}$ in Fig. 5(c) confirms relaxation peaks these relaxation peak come due to interface effect. Peaks tell us about the transition between long to short range mobility of charges. From peak broadening suggests non-Debye relaxation. Because of hydrophilic nature of $MoS_2/TiO_2$ nanocomposite this will allow water molecules to absorb on the surface which gives relaxation. When RH increases peak shifted towards higher frequency with slight decrease in height suggesting an increase in DC conductivity [28]. Peak value of M″ at each frequency is used to calculate relaxation time given by;

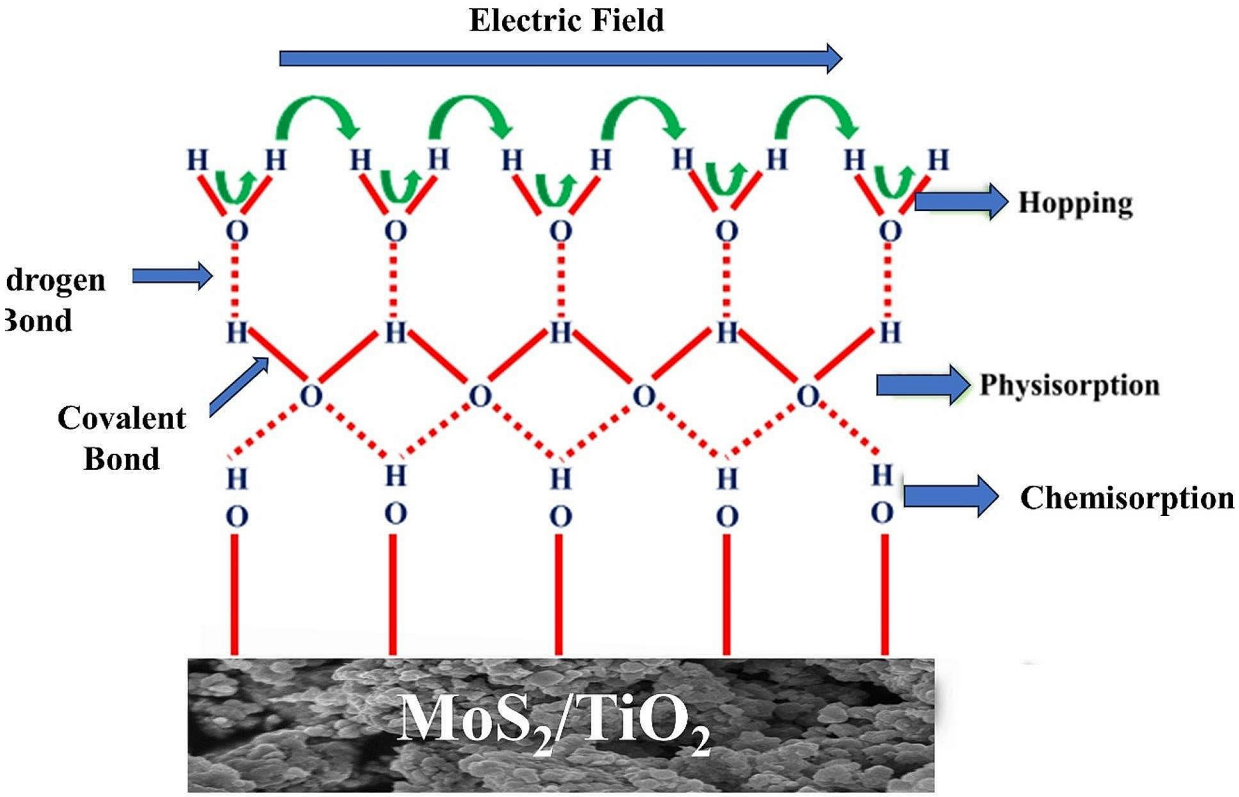


**Fig. 6** Humidity sensing schematic diagram for $MoS_2/TiO_2$ nanocomposite

$$\tau = \frac{1}{2\pi\omega_{max}} \tag{7}$$

Here $\omega_{max}$ is value of frequency at the peak value of M″. Increase in RH from 11 to 97% results in decrease in relaxation time from $2.6\times10^{-5}$s to $3.7\times10^{-6}$s.

Figure 5(d) shows Nyquist plot between M′ versus M″ at different humidity as function of frequency. The nature of curve shows asymmetric semi-circular arc whose centre lies beneath x-axis. At RH 11–97% two semi-circular arcs appearing, representing the grain and grain boundary contribution together. Nyquist plot shows incomplete semi circles which confirms single relaxation process. All the semi circles start from a common point at the lower frequency region. The coinciding semicircles at starting point for all RH show that single relaxation process occurs at higher frequency region. With increase in RH size of semi circles decreases. This may be due to fact that water adsorption on top layer of nanocomposite causes ions migration toward electrode, building a space charge at the electrode. In this frequency region ion transfer time is more than the charge transfer process, there is decrease in impedance with rise in RH.

Lastly, we explain the sensing mechanism of $MoS_2/TiO_2$ nanocomposite form the point of view of material (semi conducting, ceramic, or nanomaterial) [29]. Semiconducting behaviour and nanomaterial size play an important role in modulation of impedance with RH. Whole mechanism can be explained by Grotthuss mechanism which tell us about the conduction of proton inside the different layers of water [29]. A schematic diagram of sensing mechanism is shown in Fig. 6.

At lower RH water molecules adsorbed at the reactive sites of $MoS_2/TiO_2$ nanocomposite. Generally, SH- group is formed when water molecule interacts with sulphides. Despite this formation it is not considered experimentally

as characteristic pattern [30]. Two hydroxyls per molecule formed chemisorbed layer with $MoS_2/TiO_2$ nanocomposite and increased hydrophilic behaviour of nanocomposite. With the further raise of RH physiosorbed layer is formed. As we continue increase in RH level second physiosorbed layer making a single hydrogen bond with hydroxyl group. As a result, proton can start hopping freely through the adjacent water molecule layer and start conduction process. The proton-hopping happens conferring to the Grotthuss chain reaction ($H_2O + H_3O^+ \leftrightarrow H_3O^+ + H_2O$) [31]. No of protons increases as more and more RH increases. By lowering RH level, we can also remove physiosorbed layer. Since the experiment is conducted at ambient conditions, ionic conduction is predominant; however, when the temperature is increased, the humidity content starts to drop, and we shift from ionic conduction to electronic conduction.

## 4 Conclusions

In summary, this work explains $MoS_2/TiO_2$ nanocomposite-based humidity sensor. The $MoS_2/TiO_2$ nanocomposite was synthesised by solid state reaction method and its morphology, purity, and composition was examined using XRD, SEM and EDS. Impedance type $MoS_2/TiO_2$ nanocomposite humidity sensor was then tested from 11% RH to 97% RH. The $MoS_2/TiO_2$ nanocomposite humidity sensor shows the percentage response and sensitivity 86% and $\sim 13\ k\Omega/\%RH$, respectively. The response and recovery times of the sensor were $\sim$38s and $\sim$7s respectively with good repeatability. Moreover, the nanocomposite sensor exhibited stable response over thirty days. AC conductivity of $MoS_2/TiO_2$ nanocomposite increased with increasing RH at higher frequencies whereas it remained unaffected at lower frequencies. Complex electric modulus analysis confirmed, single relaxation process indicating that there was no electrode effect on sensor characteristics. In view of this, $MoS_2/TiO_2$ nanocomposite has potential for fabrication of humidity sensors.

### Declarations

**Competing interests** The Authors have no Competing Interests to Declare that are Relevant to the Content of this Article. No Funding was Received for Conducting this Study.

## References

1. D. Shunhao Ge, L. Sang, Y. Zou, C. Yao, H. Zhou, Fu, Hongzhu Xi, Jianchao Fan, Lijian Meng and Cong, Wang, *Nanomaterials* 2023, vol. 13, p. 1141
2. A. Burcu, Kuzubasoglu, ACS Appl. Electron. Mater. **4**, 4797–4807 (2022)
3. R. Alrammouz, J. Podlecki, A. Vena, R. Garcia, P. Abboud, R. Habchi, B. Sorli (eds.), *Sensors and Actuators B: Chemical* 2019, vol. 298, p. 126892.; (b) Hyungsub Kim, Soobin Park, Yunchan Park, Dahyun Choi, Bongyoung Yoo and Caroline Sunyong Lee, *Sensors and Actuators B: Chemical* 2018, vol. 274, pp. 331–337
4. C. Giancarla Alberti, V. Zanoni, Losi, Lisa Rita Magnaghi and Raffaela Biesuz, *Chemosensors* 2021, vol. 9, p. 108
5. A. Kumar, G. Gupta, K. Bapna, D.D. Shivagan, Mater. Res. Bull. **158**, 112053 (2023)
6. H. Indah Raya, Hamzah, Z.H. Kzar, Mahmoud, Alim Al Ayub Ahmed, Aygul Z Ibatova and Ehsan Kianfar. Carbon Lett. 2021, pp. 1–26
7. Q. Liang Huang, S. Hu, W. Gao, Liu, X. Wei, Carbohydr. Polym. 2023, p. 121139
8. V. Chauhan, J. Ram, R. Gupta, S. Kumar, P. Chaudhary, B.C. Yadav, S. Ojha, I. Sulania, R. Kumar, *Surface and Coatings Technology* 2020, vol. 392, p. 125768.; (b) Jie Ren, Bangjun Guo, Yu Feng and Ke Yu, *Physica E: Low-dimensional Systems and Nanostructures* 2020, vol. 116, p. 113782
9. X. Yu, X. Chen, X. Ding, X. Yu, X. Zhao, X. Chen, Sens. Actuators B **317**, 128168 (2020)
10. J. Jiahao Yao, W. Wang, L. Cao, M. Li, Luo, C. Wang, *Nanomaterials* 2023, vol. 13, p. 951
11. D. Zhang, X. Zong, Z. Wu, Y. Zhang, Sens. Actuators B **266**, 52–62 (2018)
12. D. Zhang, Y. Sun, P. Li, Y. Zhang, ACS Appl. Mater. Interfaces. **8**, 14142–14149 (2016)
13. H. Li, K. Yu, X. Lei, B. Guo, C. Li, H. Fu, Z. Zhu, Dalton Trans. **44**, 10438–10447 (2015)
14. G. Lu Ze, Yueqiu, Li Xujun and Zhang Yong. Appl. Surf. Sci. **399**, 330–336 (2017)
15. Debasree, Burman, Devendra Singh Choudhary and Prasanta Kumar Guha. IEEE Sens. J. **19**, 3993–3999 (2019)
16. Y. Ji Wu, W. Chen, Shen, Ying Wu and Jean-Pierre Corriou. Ceram. Int. **49**, 2204–2214 (2023)
17. A. Giampiero Montesperelli, E. Pumo, A. Traversa, Bearzotti, Angelo Montenero and Guglielmina Gnappi. Sens. Actuators B **25**, 705–709 (1995)
18. V. Bice Fubini, M. Bolis, Bailes, S. Frank, Stone, Solid State Ionics. **26**, 155–156 (1988)
19. W.-D. Lin, C.-T. Liao, T.-C. Chang, Chen and Ren-Jang Wu. Sens. Actuators B **209**, 555–561 (2015)
20. M. Gonzalo Quincot, J. Azenha, Barros, R. Faria, Univ. Minho Guimaraes Port. **1**, 1–32 (2011)
21. M.F. Afsar, M.A. Rafiq, A. Jamil, S. Fareed, Fizza Siddique, Alfred Iing Yoong Tok and Muhammad Masood Ul Hasan. ACS Omega. **4**, 2030–2039 (2019)
22. K. Muhammad Usman, S.S. Rasool, Z. Batool, M. Imran, H. Ahmad, M.A. Jamil, Rafiq, M.M. Hasan, J. Mater. Sci. Technol. **30**, 748–752 (2014)
23. B.C. Anand, R. Shashidhar, N. Choudhary, Digest J. Nanomaterials Biostructures (DJNB) 2023, **18**
24. S.S. Batool, Z. Imran, M. Israr-Qadir, S. Jamil-Rana, M. Usman, H. Jamil, M.A. Rafiq, M.M. Hasan, O. Nur, M. Willander, *Vacuum* 2013, vol. 87, pp. 1–6
25. J. Khalil, M. Hamam, Mohammad, G. Al-Amar, Mezei, Ramakrishna Guda and Clement Burns. J. Mol. Liq. **199**, 324–329 (2014)
26. S. Subhajit Maur, N. Chatterjee, P. Haque, Preetha, Sovan Dalai and Biswendu Chatterjee. IEEE Sens. J. **21**, 12236–12244 (2021)
27. M. Belal Hossen, A.K.M. Akther Hossain, J. Adv. Ceram. **4**, 217–225 (2015)
28. K. Yamamoto, H. Namikawa, Jpn. J. Appl. Phys. **27**, 1845 (1988)
29. Z. Chen, C. Lu, *Sensor letters* 2005, vol. 3, pp. 274–295
30. Paul Ratnasamy, J. Jose, Fripiat, Trans. Faraday Soc. **66**, 2897–2910 (1970)

31. K. Jiang, T. Fei, T. Zhang, RSC Adv. **4**, 43189–43194 (2014)
32. B. Zhao, J.-S. Wang, J. Zheng, Y. Wu, C.-C. Wang, Mater. Lett. **330**, 133345 (2023)
33. L.S. Dalibor, B. Tamara, S. Ivetić, 2023, vol. 23, p. 8261